Geophysical Research Letters

RESEARCH LETTER
10.1029/2025GL121001

Can Terrain Induce Moist Absolutely Unstable Layers and Enhance Extreme Rainfall?

Jyong-En Miao[1,2], Ming-Jen Yang[1], Kristen L. Rasmussen[3], and Michael M. Bell[3]

[1]Department of Atmospheric Sciences, National Taiwan University, Taipei, Taiwan, [2]Now at Max Planck Institute for Meteorology, Hamburg, Germany, [3]Department of Atmospheric Science, Colorado State University, Fort Collins, CO, USA

Key Points:

- Terrain lifting generated moist absolutely unstable layers associated with extreme orographic rainfall
- Topography promoted deep instability through sustained layer lifting and enhanced low-level moisture convergence
- The volume of the moist absolutely unstable layer increased rapidly prior to the onset of the most intense precipitation

Supporting Information:

Supporting Information may be found in the online version of this article.

Correspondence to:

J.-E. Miao,
jjackm123@gmail.com

Citation:

Miao, J.-E., Yang, M.-J., Rasmussen, K. L., & Bell, M. M. (2026). Can terrain induce moist absolutely unstable layers and enhance extreme rainfall? *Geophysical Research Letters*, *53*, e2025GL121001. https://doi.org/10.1029/2025GL121001

Received 1 DEC 2025
Accepted 25 MAR 2026

Author Contributions:

Conceptualization: Jyong-En Miao, Ming-Jen Yang, Kristen L. Rasmussen, Michael M. Bell
Data curation: Jyong-En Miao
Formal analysis: Jyong-En Miao
Funding acquisition: Jyong-En Miao, Ming-Jen Yang
Investigation: Jyong-En Miao, Ming-Jen Yang, Kristen L. Rasmussen, Michael M. Bell
Methodology: Jyong-En Miao, Ming-Jen Yang, Kristen L. Rasmussen, Michael M. Bell
Project administration: Ming-Jen Yang, Kristen L. Rasmussen
Resources: Ming-Jen Yang, Kristen L. Rasmussen

Abstract Extreme rainfall events in Taiwan pose significant forecasting challenges due to complex multiscale interactions. Although orographic lifting is known to trigger convection, its role in modifying atmospheric stability, specifically through the formation of moist absolutely unstable layers (MAULs), remains underexplored. This study presents the first investigation demonstrating that terrain can induce MAULs and enhance extreme rainfall in mountainous terrain in Taiwan, a mechanism not previously documented. Convection-permitting simulations show that terrain-driven moisture convergence and layer lifting promote deeper and more persistent MAULs. Removing the terrain substantially limits the MAUL development, associated with weaker rainfall. Furthermore, the MAUL volume rapidly increases prior to the most intense rainfall, suggesting its potentital as an indicator of extreme precipitation. These findings highlight the role of terrain in modulating both the thermodynamic environment and extreme rainfall, underscoring the importance of accurately representing orographic effects in numerical weather prediction.

Plain Language Summary Extreme rainfall in mountainous regions, such as Taiwan, poses a significant threat to life and property, yet predicting exactly when and where these storms will strike remains difficult. In this study, we investigated how complex topography influences the formation of severe storms. Using high-resolution computer simulations of a heavy rainfall event, we found that mountains did more than just block the wind; they acted like a ramp that forces moist air to rise in a deep, continuous layer. This process created a highly unstable atmospheric condition known as a "Moist Absolutely Unstable Layer" (MAUL). Our results show that this mountain-induced instability was associated with explosive storm growth. When we removed the mountains in our simulation, this unstable layer could not form effectively, and the rainfall was much weaker. Crucially, we found that the size of this unstable layer grew rapidly just before the heaviest rain began. This suggests that monitoring this specific type of instability could help meteorologists better predict extreme rainfall events in the future.

1. Introduction

Terrain plays a fundamental role in modulating moist convection and extreme rainfall (Houze, 2012). While previous studies have focused on the mechanical effects of orographic lifting on initiating deep convection on a global scale (e.g., Antonelli & Rotunno, 2025; Caracena et al., 1979; Du et al., 2020; Maddox et al., 1978; Miao & Yang, 2020; Miao & Yang, 2022; Rasmussen & Houze, 2012), the specific role of complex topography in modifying the thermodynamic environment remains less understood. Beyond its mechanical effects, orographic lifting can destabilize the atmosphere by lifting moist, conditionally unstable air to saturation, forming moist absolutely unstable layers (MAULs; Bryan & Fritsch, 2000)—saturated layers where the lapse rate exceeds the moist adiabatic rate, promoting rapid convective growth (Bryan & Fritsch, 2000; Kirshbaum et al., 2018).

A growing number of observational and modeling studies (Table S1 in Supporting Information S1) have identified the presence of MAULs in a variety of storm environments across different geographic regions. Bryan and Fritsch (2000) and Mechem et al. (2002) highlighted MAULs within MCSs over the midlatitude United States and the tropical western Pacific, respectively. In both studies, the MAULs extended horizontally for hundreds of kilometers along the axis of mesoscale convective systems (MCSs) and vertically up to ~100 mb, primarily formed by mesoscale lifting induced by cold pools. Takemi (2007) further noted that MAULs facilitated new cell generation at the leading edge of simulated squall lines. Schumacher and Johnson (2008) similarly found deep (~1–2 km) MAULs in flash-flood-producing MCSs, associated with mesoscale convective vortices. Zou

Software: Jyong-En Miao
Supervision: Ming-Jen Yang, Kristen L. Rasmussen
Validation: Jyong-En Miao
Visualization: Jyong-En Miao
Writing – original draft: Jyong-En Miao
Writing – review & editing: Ming-Jen Yang, Kristen L. Rasmussen, Michael M. Bell

et al. (2023) found MAULs within a narrow cold frontal rainband associated with an atmospheric river in California, driven by large-scale frontal convergence.

Recently, MAULs have been documented in several heavy rainfall events in East Asia. Choi et al. (2011) found deep (~200 mb) MAULs aligned along linear MCSs in the Korean Peninsula, maintained by strong vertical motion due to the presence of a low-level jet. Takemi and Unuma (2020) analyzed Typhoon Hagibis (2019) and identified MAULs over 2 km deep in eastern Japan, associated with abundant moisture and the circulation of the typhoon. Tsuji et al. (2021) examined moisture transport during heavy rainfall events in western Japan and indicated that a MAUL was present in the mid-to-lower troposphere around the time of peak precipitation, occurring more frequently during intense rainfall. Hua et al. (2020) examined a heavy rainfall event in the mountainous region of North China and revealed shallow MAULs (<1 km) generated by orographic gravity waves.

Although some research has hinted at a possible link between terrain and MAULs (Hua et al., 2020; Takemi & Unuma, 2020), the role of terrain in inducing MAULs and enhancing localized extreme rainfall has not been explicitly demonstrated and explored. This knowledge gap is particularly significant for Taiwan, a region characterized by steep topography, tropical moisture, and frequent low-level jets. To our knowledge, no prior studies have investigated the role of MAULs during heavy rainfall events in Taiwan. This study addresses this gap by investigating the hypothesis that terrain can induce MAUL formation and enhance extreme orographic rainfall. Using high-resolution numerical simulations of an extreme rainfall event over northern Taiwan during the Taiwan-Area Heavy rain Observation and Prediction Experiment/Prediction of Rainfall Extremes Campaign In the Pacific (TAHOPE/PRECIP) IOP 2, we demonstrate for the first time that terrain-forced mesoscale lifting is a crucial mechanism for generating deep and persistent MAULs that characterize the environment for extreme precipitation.

2. Case Overview and Numerical Experiments

2.1. Case Overview

This study investigates an extreme rainfall event that occurred over complex terrain during the TAHOPE/PRECIP IOP 2. Overall, this event unfolded within a strongly forced regime featuring southwesterly flow and a frontal boundary near northern Taiwan (Miao et al., 2025). Figure S1 in Supporting Information S1 shows a moist environment: 700-hPa RH exceeded 80% over the ocean north of Taiwan and ~70% inland. At 850 and 925 hPa, prevailing southwesterly monsoonal winds transported high-θ_e air (>342 K) toward Taiwan, where a leeside low pressure was observed northeast of the island.

The heaviest rainfall occurred along the Snow Mountain Range (SMR; see Figure 1 in Miao et al., 2025), with 12-hr accumulations exceeding 150 mm (Figure S1e in Supporting Information S1). Additional heavy rainfall was also observed along the eastern coastal region. Since this study focuses on orographic extreme rainfall over the SMR, Figure S2 in Supporting Information S1 presents Hovmöller diagrams of column-maximum radar reflectivity along and across the SMR. As noted by Miao et al. (2025), two main convective episodes occurred during this event: 12–14 LST and 15–17 LST. The intense convection remained confined to the mountainous terrain, while the radar echo was much weaker over the Taipei Basin.

2.2. Numerical Model Configuration and Validation

This study employs the Advanced Research version of the Weather Research and Forecasting (WRF-ARW) Model, version 4.5.2 (Skamarock et al., 2019), to simulate this extreme rainfall event over northern Taiwan. A two-way nested domain configuration is used, consisting of three domains with horizontal grid spacings of 13.5, 4.5, and 1.5 km, respectively (Figure S3 in Supporting Information S1). The model uses 55 vertically stretched levels and a model top at 20 hPa. The outermost domain employs a time step of 15 s. The simulation period spans from 1200 UTC 30 May to 1200 UTC 31 May 2022. Model outputs at intervals of 10 min are used for analyses, except for the trajectory analysis, which utilizes 5-min output data.

Physical parameterizations include the Kain–Fritsch cumulus scheme (Kain & Fritsch, 1993) applied only to the outermost domain (Δx = 13.5 km), the WDM6 microphysics scheme (Lim & Hong, 2010), the Rapid Radiative Transfer Model (RRTM) for longwave radiation (Mlawer et al., 1997), the Dudhia (1989) scheme for shortwave radiation, and the Yonsei University (YSU) planetary boundary layer scheme (Hong & Pan, 1996). Initial and

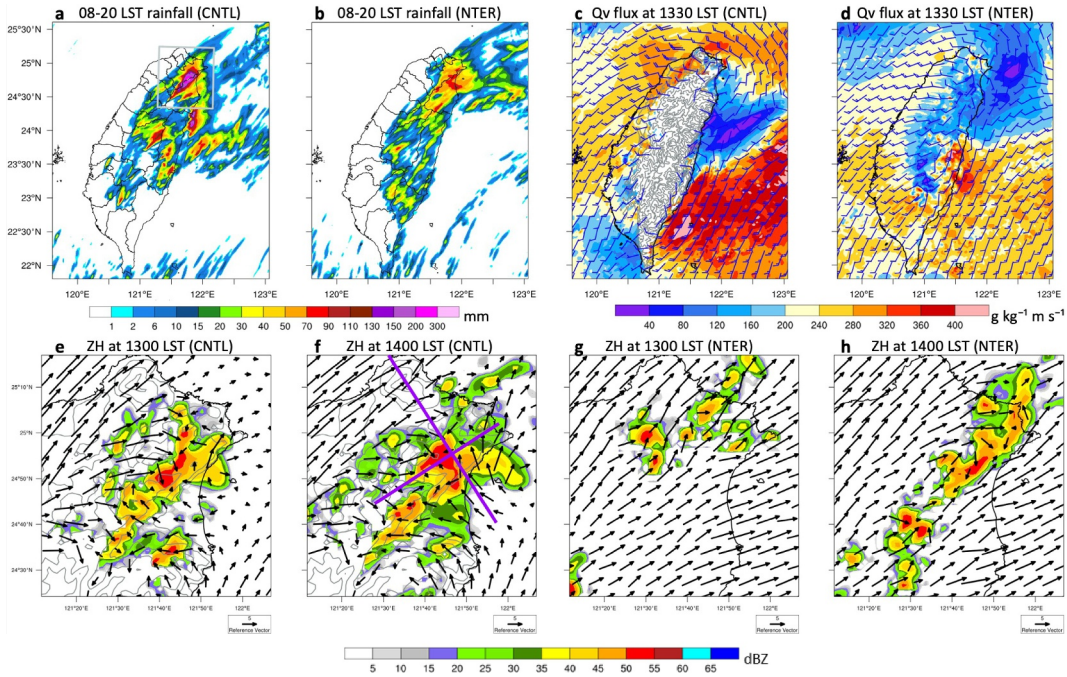

Figure 1. 0800–2000 LST accumulated rainfall (mm) from the (a) CNTL (the gray box indicates the northern Taiwan domain) and (b) NTER simulations. 0.5-km moisture flux (colored; unit: g kg^{-1} m s^{-1}) and horizontal wind (barbs; full barb is 10 kt, half barb is 5 kt) at 1330 LST for (c) CNTL and (d) NTER. Terrain heights are contoured by gray lines at 100, 300, 700, 1,300, 2,000, and 2,500 m. Simulated 1.5-km radar reflectivity (colored; unit: dBZ) and horizontal winds (vectors) for CNTL at (e) 1300 LST and (f) 1400 LST, and for NTER at (g) 1300 LST and (h) 1400 LST. Terrain heights are contoured by gray lines at 100, 300, 700, and 1,300 m. The purple lines in (f) indicate NW–SE and NE–SW cross sections used for analyses. The northern Taiwan domain in (e)–(h) covers a spatial extent of approximately 84 km × 92 km.

lateral boundary conditions were provided by the NCEP Final (FNL) Operational Global Analysis data, available every 6 hr with a horizontal resolution of 0.25°.

The control (CNTL) simulation demonstrates reasonable skill in capturing the synoptic to mesoscale environment associated with this event (Figures S1 and S4 in Supporting Information S1). It reproduces the moist region (RH >70%) near northern Taiwan at 700 hPa, which is consistent with the reanalysis. The simulation also captures the low-level southwesterly flow transporting high-θ_e air toward Taiwan, the formation of a leeside low pressure northeast of the island, and the position of the surface front offshore of northern Taiwan. While the CNTL underestimates the light rainfall along the western coast, it successfully captures the heavy rainfall over the northern mountainous region and eastern coastal area (Figure 1a and Figure S1e in Supporting Information S1). In addition, the simulated convection evolution over the terrain aligns with observations (Figures S2 and S5 in Supporting Information S1), reproducing the two distinct convective episodes and the confinement of strong reflectivity over the SMR. These results indicate that the CNTL reasonably captures the key features of the event, providing a reliable framework for investigating the role of terrain in MAUL formation and extreme orographic rainfall. To further examine the effects of terrain, a sensitivity experiment without Taiwan's topography (NTER) was conducted using identical model configurations as the CNTL, except for the terrain height. In the NTER experiment, the topography of the Taiwan island was modified to 0 m AMSL across all nested domains to ensure consistency, and the land-use categories were kept identical to those in the CNTL simulation.

2.3. Moisture Flux Convergence

Moisture flux convergence (MFC) is a widely used diagnostic tool for evaluating atmospheric conditions favorable for convective initiation and development (Banacos & Schultz, 2005; Rasmussen & Houze, 2016; Wu et al., 2020). Following Banacos and Schultz (2005), MFC is calculated with the formula,

$$MFC = -u\frac{\partial q}{\partial x} - v\frac{\partial q}{\partial y} - q\left(\frac{\partial u}{\partial x} + \frac{\partial v}{\partial y}\right)$$

where u and v represent the zonal and meridional wind components, respectively, and q denotes the specific humidity. The first two terms correspond to the horizontal advection of moisture, and the third term represents the moisture increase by wind convergence. In this study, we calculate the vertically integrated MFC from 0 to 3 km above mean sea level (AMSL). Spatial averages are computed over the northern Taiwan domain (Figure 1e).

2.4. MAUL Identification and MAUL Volume

Following Takemi and Unuma (2020), a MAUL is defined where $\partial\theta_e/\partial z < 0$ and RH > 99%, with θ_e calculated according to Bolton (1980; Equation 39). To quantify its total extent, we calculate the MAUL volume in the northern Taiwan domain. First, for each grid column, we determine the total MAUL depth by summing all contiguous vertical segments that satisfy the MAUL criteria and span at least three model levels. This specific constraint is introduced to filter out shallow instability in the high-resolution simulation. The MAUL volume is then computed by integrating the depths of only those columns where the total MAUL depth exceeds 0.5 km to effectively isolate physically significant instability (Naka & Takemi, 2023, 2025).

3. Results

3.1. Terrain Enhanced MFC and Induced MAUL Over Northern Taiwan

The CNTL simulation produces intense, localized rainfall along the Snow Mountain Range (SMR), with a maximum accumulation of ∼200 mm (Figure 1a). In contrast, the NTER experiment simulates substantially weaker and more scattered rainfall over northern Taiwan, with a peak accumulation of only ∼90 mm and significantly reduced coastal rainfall (Figure 1b).

A key question is how the terrain influences the development of this extreme orographic rainfall event under the prevailing southwesterly monsoon flow. The CNTL simulation shows strong low-level moisture flux over northern Taiwan (maximum ∼320 g kg^{-1} m s^{-1}; Figure 1c). Located within the wake region of the southwesterly monsoon flow, northern Taiwan experiences enhanced moisture transport, where the wake flow interacts with sea breeze and upslope winds (Figures S6–S8 in Supporting Information S1), channeling moisture toward the SMR. In contrast, the NTER experiment simulates a much weaker moisture flux over northern Taiwan (∼160 g kg^{-1} m s^{-1}; Figure 1d), and this contrast is consistent across heights and times (Figures S6 and S7 in Supporting Information S1). Moreover, the CNTL captures a convergence line offshore of eastern Taiwan, with intensified moisture flux along its southern flank, while the NTER fails to reproduce this feature and shows a considerably weaker flux magnitude (Figures 1c and 1d). These differences underscore the critical role of terrain in redistributing and intensifying moisture transport under a southwesterly monsoon regime.

Extreme rainfall can result from high rainfall intensity, prolonged rainfall duration, or a combination of both factors. Thus, it is crucial to discuss the role of terrain in both of these processes (Cornejo et al., 2024; Doswell et al., 1996). Figures 1e and 1f show that low-level convergence associated with upslope flow develops along the SMR, supporting convection development and confining strong convection over the terrain (Figure S5 in Supporting Information S1), which is consistent with the observational findings of Miao et al. (2025). In NTER, the southwesterly monsoon flow penetrates into northern Taiwan (Figures 1g and 1h), and once convection forms, it propagates southeastward following a sea-breeze-induced convergence line toward the ocean. The absence of terrain in NTER leads to more transient convection with fast propagation, highlighting the role of orography in maintaining persistent deep convection over the SMR.

In support of the preceding discussion, Table S2 in Supporting Information S1 presents the time-averaged, vertically integrated (0–3 km AMSL) MFC over northern Taiwan. The CNTL run exhibits a value of 44.5×10^4 kg s^{-1} m^{-2}, approximately 18% higher than NTER (37.8×10^4 kg s^{-1} m^{-2}), with both simulations showing dominance of the wind convergence term. This result indicates the role of terrain in enhancing low-level moisture accumulation and promoting a more humid environment over northern Taiwan (Figure S9 in Supporting Information S1).

10.1029/2025GL121001

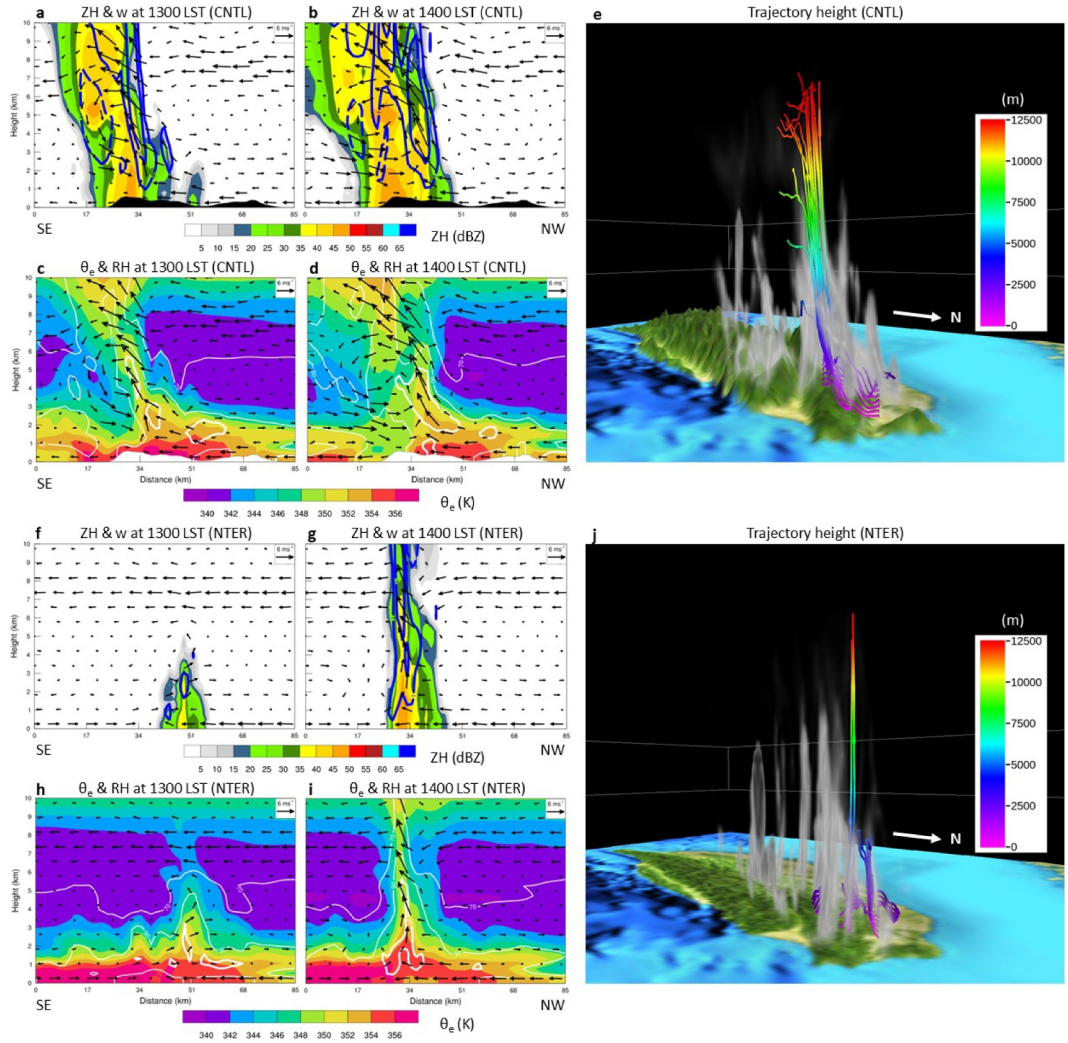

Figure 2. (a–d) The northwest-southeast cross sections (location shown in Figure 1f) for the CNTL simulation, averaged over a 15-km width. (a, b) Radar reflectivity (colored), vertical velocity (blue contoured at −1, 1, 3, and 6 m s^{-1}; dashed line for downdraft), and airflow (vectors). (c, d) Equivalent potential temperature (colored), relative humidity (white contoured at 70%, 90%, and 99%), and airflow (vectors). (e) 60-min forward trajectories initialized at 1300 LST in the CNTL simulation, colored by height (m). (f–j) As in (a–e), but for the NTER simulation.

To examine the convective structure, Figure 2 presents vertical cross sections of simulated radar reflectivity and equivalent potential temperature (θ_e) along a southeast–northwest cross section. In the CNTL simulation (Figures 2a and 2b), convection initiates over the SMR by 1200 LST and rapidly intensifies (not shown), with 40-dBZ reflectivity extending upward to 9–10 km by 1300–1400 LST. This convective structure is associated with persistent upslope flow and strong updrafts ($w > 6$ m s^{-1}). The ascending inflow forms a ∼2-km-deep layer of $\theta_e > 352$ K (Figures 2c and 2d), associated with the development of MAULs (regions with $\partial\theta_e/\partial z < 0$ and RH > 99%) over the slope region. These MAULs are pronounced during 1300–1400 LST and are accompanied by intense convection and updrafts. The CNTL simulation exhibits features similar to the MAUL conceptual model proposed by Bryan and Fritsch (2000; their Figure 5), including a potentially unstable environment in the mid-to-lower troposphere, the presence of MAULs near the inflow region, and the intrusion of descending low-θ_e air from the opposite side of the inflow into the convection.

In contrast, the NTER simulation shows markedly shallower convection (Figures 2f and 2g), with 40-dBZ reflectivity reaching a height of only 4 km and weaker updrafts. The θ_e structure in NTER (Figures 2h and 2i) indicates a thinner layer of inflow (∼1 km). MAULs are also less extensive in NTER, suggesting that the absence of terrain suppresses the formation of deep and broad MAULs.

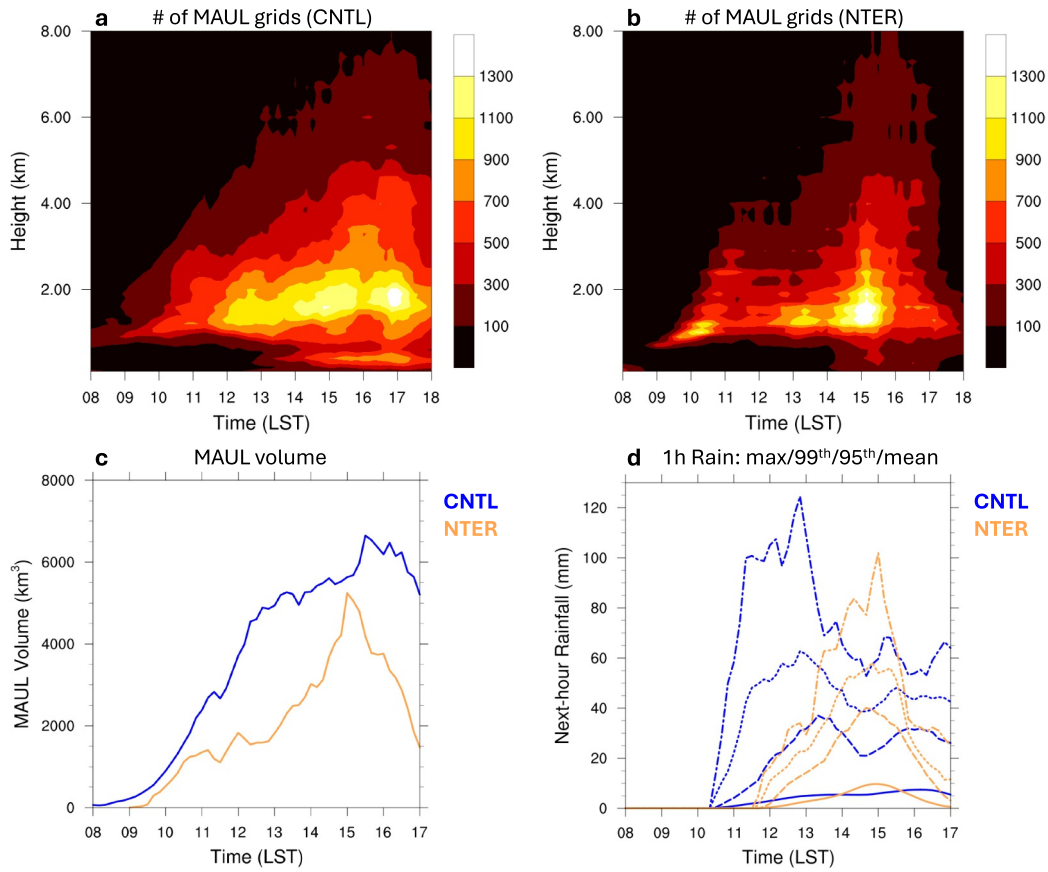

Figure 3. Temporal evolution of MAUL and its relationship with subsequent rainfall in the northern Taiwan domain (domain is shown in Figure 1e). Time-height diagrams showing the number of MAUL grids at each level for the (a) CNTL and (b) NTER simulations. Note that each grid cell represents a horizontal area of 2.25 km^2. (c) Time series of the total MAUL volume (km^3) for CNTL (blue line) and NTER (orange line). (d) Time series of next-hour rainfall statistics (mm), comparing CNTL (blue lines) and NTER (orange lines). Line styles represent the maximum (dash-dotted), 99th percentile (dotted), 95th percentile (dashed), and domain-averaged (solid) rainfall.

Previous research on MAULs suggests that these unstable layers are often associated with layer-lifting inflow (Bryan & Fritsch, 2000; Mechem et al., 2002). To further examine the impact of Taiwan's topography on the nature of inflow ascent, 60-min forward trajectories were initialized at 1300 LST. These trajectories were calculated and plotted using the Visualization and Analysis Platform for Atmospheric, Oceanic and Solar Research (VAPOR; Clyne & Rast, 2005; Clyne et al., 2007) software. In the CNTL, tracers originating from the Taipei Basin are lifted upslope as a coherent layer, with most tracers reaching the upper level (Figure 2e). In contrast, the NTER exhibits a parcel-based ascent pattern, where only near-surface tracers are lifted, and the majority remain below 5 km (Figure 2j). These results suggest that terrain facilitates layer lifting conducive to MAUL formation and promotes the development of deep convection, noting the potential smoothing on the trajectory due to the 5-min model output resolution.

3.2. The Relationship Between MAUL and Extreme Rainfall

Figures 3a and 3b show time–height plots of MAUL grid counts within the northern Taiwan domain, where the count at each level represents the horizontal area coverage. It is evident that the CNTL produces broader and deeper MAUL structures, with the 500-grid contour (corresponding to a horizontal area of ∼1,125 km^2) extending from near the surface up to ∼5 km (Figure 3a). In contrast, the NTER shows more limited MAUL coverage, largely confined between 1 and 3.5 km (Figure 3b). Notably, only the CNTL exhibits significant MAUL presence below 1 km after 1300 LST, consistent with the enhanced relative humidity (Figure S9 in Supporting

Information S1). These results again highlight the important role of terrain-enhanced MFC in sustaining deep and persistent MAULs.

To further examine the relationship between MAUL and extreme rainfall, Figures 3c and 3d show a time series of MAUL volume and next-hour rainfall over land within the northern Taiwan domain. In the CNTL, the MAUL volume begins increasing rapidly after 0900 LST, exceeds 2,000 km^3 around 1100 LST, and reaches over 6,500 km^3 by 1530 LST (Figure 3c). In contrast, the NTER exhibits a more gradual increase, with the MAUL volume surpassing 2,000 km^3 around 1300 LST and a lower peak of ∼5,000 km^3 by 1500 LST. Correspondingly, extreme rainfall in the CNTL occurs earlier and is more intense than in the NTER (Figure 3d). For example, the maximum 1-hr rainfall in the CNTL (∼125 mm) peaks nearly 2 hr earlier than in the NTER (∼100 mm). A similar pattern is observed in the 99th percentile rainfall, whereas the 95th percentile maxima are comparable between the simulations. The domain-average rainfall peak is marginally higher in the NTER. These differences indicate that the maximum rainfall in the CNTL is more spatially concentrated over the SMR (Figure 1a; ∼200 mm), while the NTER exhibits a broader distribution (Figure 1b; ∼90 mm), suggesting that terrain confines convection to mountainous regions and enhances localized extreme precipitation.

Notably, the analysis reveals that significant MAUL development precedes heavy precipitation in this case. In both CNTL and NTER, the MAUL volume begins to increase rapidly 1–2 hr before the peak rainfall rates are observed (Figures 3c and 3d). We also note a tendency for intense rainfall rates (>40 mm/hr) to occur only after the MAUL volume has become substantial (Figure S10 in Supporting Information S1). This temporal relationship suggests that MAUL development may serve as an indicator of a thermodynamic environment favorable for extreme precipitation.

4. Summary and Discussion

This study provides the first investigation of how terrain induces MAULs and enhances extreme rainfall in Taiwan. Using convection-permitting simulations (Δx = 1.5 km), we show that Taiwan's topography plays a critical role in enhancing low-level MFC in the wake region of the southwesterly monsoon. Specifically, the interaction of the wake flow with sea breeze and upslope winds transports abundant moisture toward the mountains, where orographic layer lifting generates deep and persistent MAULs. This physical mechanism, summarized in Figure 4, contrasts sharply with the weaker parcel-based convection seen in simulations without terrain, highlighting that terrain-induced MAULs characterize a thermodynamic environment favorable for extreme precipitation.

Our findings extend the classical understanding of MAUL formation by identifying orographic layer lifting as a crucial and previously underexplored pathway, particularly in tropical, moisture-rich environments. While prior research has established the necessity of dynamically forced mesoscale ascent for sustaining MAULs, it has largely focused on other mechanisms like cold pool lifting (Bryan et al., 2007; Bryan & Fritsch, 2000; Mechem et al., 2002). Our results demonstrate that terrain-modulated flows provide a dual contribution: they supply the necessary dynamical ascent while simultaneously enhancing the local MFC. This synergy creates a more humid environment that is conducive to moist absolute instability (Mechem et al., 2002; Takemi & Unuma, 2020; Tsuji et al., 2021), facilitating the deep MAULs associated with the orographic extreme rainfall.

The results underscore the diagnostic potential of the MAUL as an indicator of extreme rainfall, as its occurrence is associated with precipitation intensification. Our analysis reveals that the rapid growth of the MAUL volume precedes the most intense rainfall, consistent with the suggested causal links in Naka and Takemi (2025). While orographic lifting provides the primary mechanical trigger, the emergence of a MAUL likely facilitates a structural transition from discrete cellular convection to a slab-like overturning mode, potentially enhancing precipitation intensity (Takemi, 2007). Given that our simulations are convection-permitting, detailed overturning morphology should be interpreted qualitatively and may be resolution dependent (Bryan et al., 2003).

Although this study focuses on a single case, the process-based insights lay the groundwork for a broader investigation. Future research should assess the generality of these findings across multiple events and incorporate high-resolution observations to validate the simulated MAUL structures and their relationships with precipitation (e.g., Naka & Takemi, 2025; Tsuji et al., 2021). Furthermore, evaluating the representation of these terrain-MAUL dynamics in operational weather and regional climate models will be essential for improving the prediction of high-impact weather over complex terrain.

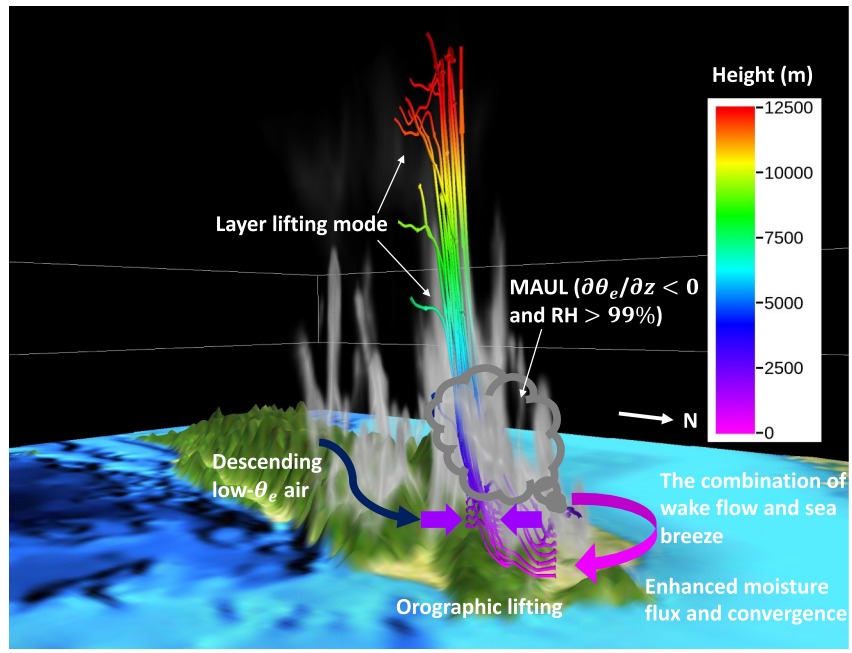

Figure 4. Conceptual model illustrating the formation of terrain-induced MAUL and the enhancement of orographic rainfall. The interaction of the background southwesterly flow with Taiwan's topography creates a wake region where the combination of wake flow and sea breeze enhances low-level moisture flux and convergence. This moisture-rich air is then forced upward along the mountain slope in a pronounced layer-lifting mode. Sustained ascent leads to the formation of a deep MAUL, creating a thermodynamically favorable environment for deep convection and extreme rainfall.

Conflict of Interest

The authors declare no conflicts of interest relevant to this study.

Availability Statement

The S-Pol radar observations analyzed in this study can be accessed through the NCAR Earth Observing Laboratory repository (NCAR/EOL S-Pol Team, 2023) at https://doi.org/10.26023/QA4M-CDHH-MY0Z. The FNL reanalysis data used in this study are available from the NCAR's Data Support Section at https://gdex.ucar.edu/datasets/d083003 (NCEP, 2015). The Advanced Research version of the Weather Research and Forecasting (WRF-ARW) Model (version 4.5.2) is available from https://www.mmm.ucar.edu/models/wrf. The WRF namelists used in this study are available at Zenodo via https://doi.org/10.5281/zenodo.17777774 (Miao, 2025). The Visualization and Analysis Platform for Atmospheric, Oceanic and Solar Research (VAPOR) software can be downloaded from https://www.vapor.ucar.edu.

Acknowledgments
The authors thank the participants of the TAHOPE/PRECIP/T-PARCII campaigns for their dedicated efforts in data collection. We also appreciate the constructive comments from the anonymous reviewers, which significantly improved the manuscript. Numerical simulations were performed on the Derecho supercomputer at the National Center for Atmospheric Research (NCAR). J.-E. Miao was supported by the National Science and Technology Council (NSTC) of Taiwan under the Graduate Students Study Abroad Program (NSTC 113-2917-I-002-051) during his research visit to Colorado State University, and by the Postdoctoral Fellowship (NSTC 114-2811-M-002-165). M.-J. Yang was supported by NSTC Grant 114-2111-M-002-013. K. L. Rasmussen was supported by NSF Grant AGS-1854399. M. M. Bell was supported by NASA award 80NSSC23K1306.

References

Antonelli, M., & Rotunno, R. (2025). Effect of orography on deep convection initiation produced by two sea-breeze fronts. *Journal of the Atmospheric Sciences*, *82*(10), 2219–2236. https://doi.org/10.1175/JAS-D-24-0254.1

Banacos, P. C., & Schultz, D. M. (2005). The use of moisture flux convergence in forecasting convective initiation: Historical and operational perspectives. *Weather and Forecasting*, *20*(3), 351–366. https://doi.org/10.1175/WAF858.1

Bolton, D. (1980). The computation of equivalent potential temperature. *Monthly Weather Review*, *108*(7), 1046–1053. https://doi.org/10.1175/1520-0493(1980)108<1046:TCOEPT>2.0.CO;2

Bryan, G. H., & Fritsch, J. M. (2000). Moist absolute instability: The sixth static stability state. *Bulletin of the American Meteorological Society*, *81*(6), 1207–1230. https://doi.org/10.1175/1520-0477(2000)081<1287:maitss>2.3.co;2

Bryan, G. H., Rotunno, R., & Fritsch, J. M. (2007). Roll circulations in the convective region of a simulated squall line. *Journal of the Atmospheric Sciences*, *64*(4), 1249–1266. https://doi.org/10.1175/JAS3899.1

Bryan, G. H., Wyngaard, J. C., & Fritsch, J. M. (2003). Resolution requirements for the simulation of deep moist convection. *Monthly Weather Review*, *131*(10), 2394–2416. https://doi.org/10.1175/1520-0493(2003)131<2394:RRFTSO>2.0.CO;2

Caracena, F., Maddox, R. A., Hoxit, L. R., & Chappell, C. F. (1979). Mesoanalysis of the big Thompson storm. *Monthly Weather Review*, *107*, 1–17. https://doi.org/10.1175/1520-0493(1979)107<0001:motbts>2.0.co;2

Choi, H.-Y., Ha, J.-H., Lee, D.-K., & Kuo, Y.-H. (2011). Analysis and simulation of mesoscale convective systems accompanying heavy rainfall: The Goyang case. *Asia-Pacific Journal of Atmospheric Sciences*, *47*(3), 265–279. https://doi.org/10.1007/s13143-011-0015-x

Clyne, J., Mininni, P., Norton, A., & Rast, M. (2007). Interactive desktop analysis of high-resolution simulations: Application to turbulent plume dynamics and current sheet formation. *New Journal of Physics*, *9*(8), 301. https://doi.org/10.1088/1367-2630/9/8/301

Clyne, J., & Rast, M. (2005). A prototype discovery environment for analyzing and visualizing terascale turbulent fluid flow simulations. In *Proceedings of visualization and data analysis* (pp. 284–294).

Cornejo, I. C., Rowe, A. K., Rasmussen, K. L., & DeHart, J. C. (2024). Orographic controls on extreme precipitation associated with a Mei-Yu front. *Monthly Weather Review*, *152*(2), 531–551. https://doi.org/10.1175/MWR-D-23-0170.1

Doswell, C. A., Brooks, H. E., & Maddox, R. A. (1996). Flash flood forecasting: An ingredients-based methodology. *Weather and Forecasting*, *11*(4), 560–581. https://doi.org/10.1175/1520-0434(1996)011<0560:fffaib>2.0.co;2

Du, Y., Chen, G., Han, B., Bai, L., & Li, M. (2020). Convection initiation and growth at the coast of south China. Part II: Effects of the terrain, coastline, and cold pools. *Monthly Weather Review*, *148*(9), 3871–3892. https://doi.org/10.1175/MWR-D-20-0090.1

Dudhia, J. (1989). Numerical study of convection observed during the winter monsoon experiment using a mesoscale two-dimensional model. *Journal of the Atmospheric Sciences*, *46*(20), 3077–3107. https://doi.org/10.1175/1520-0469(1989)046<3077:nsocod>2.0.co;2

Hong, S.-Y., & Pan, H.-L. (1996). Nonlocal boundary layer vertical diffusion in a medium-range forecast model. *Monthly Weather Review*, *124*(10), 2322–2339. https://doi.org/10.1175/1520-0493(1996)124<2322:nblvdi>2.0.co;2

Houze, R. A., Jr. (2012). Orographic effects on precipitating clouds. *Reviews of Geophysics*, *50*(1), RG1001. https://doi.org/10.1029/2011RG000365

Hua, S., Xu, X., & Chen, B. (2020). Influence of multiscale orography on the initiation and maintenance of a precipitating convective system in North China: A case study. *Journal of Geophysical Research: Atmospheres*, *125*(13), e2019JD031731. https://doi.org/10.1029/2019jd031731

Kain, J. S., & Fritsch, J. M. (1993). Convective parameterization for mesoscale models: The Kain-Fritsch scheme. In *The representation of cumulus convection in numerical models*. In *Meteorological Monographs* (Vol. 46, pp. 165–177). American Meteor Society.

Kirshbaum, D. J., Adler, B., Kalthoff, N., Barthlott, C., & Serafin, S. (2018). Moist orographic convection: Physical mechanisms and links to surface-exchange processes. *Atmosphere*, *9*(3), 80. https://doi.org/10.3390/atmos9030080

Lim, K.-S. S., & Hong, S.-Y. (2010). Development of an effective double-moment cloud microphysics scheme with prognostic cloud condensation nuclei (CCN) for weather and climate models. *Monthly Weather Review*, *138*(5), 1587–1612. https://doi.org/10.1175/2009mwr2968.1

Maddox, R. A., Hoxit, L. R., Chappell, C. F., & Caracena, F. (1978). Comparison of meteorological aspects of the Big Thompson flood and Rapid City flash floods. *Monthly Weather Review*, *106*(3), 375–389. https://doi.org/10.1175/1520-0493(1978)106<0375:comaot>2.0.co;2

Mechem, D. B., Houze, R. A., Jr., & Chen, S. S. (2002). Layer inflow into precipitating convection over the western tropical Pacific. *Quarterly Journal of the Royal Meteorological Society*, *128*(584), 1997–2030. https://doi.org/10.1256/003590002320603502

Miao, J.-E. (2025). Supporting Data for: GRL manuscript "Can terrain induce moist absolutely unstable layers and enhance extreme rainfall?" [Dataset]. *Zenodo*. https://doi.org/10.5281/zenodo.17777774

Miao, J.-E., & Yang, M.-J. (2020). A modeling study of the severe afternoon thunderstorm event at Taipei on 14 June 2015: The roles of sea breeze, microphysics, and terrain. *Journal of the Meteorological Society of Japan*, *98*(1), 129–152. https://doi.org/10.2151/jmsj.2020-008

Miao, J.-E., & Yang, M.-J. (2022). The impacts of midlevel moisture on the structure, evolution, and precipitation of afternoon thunderstorms: A real-case modeling study at Taipei on 14 June 2015. *Journal of the Atmospheric Sciences*, *79*(7), 1837–1857. https://doi.org/10.1175/JAS-D-21-0257.1

Miao, J.-E., Yang, M.-J., Rasmussen, K. L., Bell, M. M., Kuo, H.-C., & Cha, T.-Y. (2025). Microphysical and kinematical characteristics of merged and isolated convective cells over the complex terrain of the Taipei Basin. *Journal of Geophysical Research: Atmospheres*, *130*(15), e2024JD042375. https://doi.org/10.1029/2024JD042375

Mlawer, E. J., Taubman, S. J., Brown, P. D., Iocono, M. J., & Clough, S. A. (1997). Radiative transfer for inhomogeneous atmospheres: RRTM, a validated correlated-k model for the longwave. *Journal of Geophysical Research*, *102*(D14), 16663–16682. https://doi.org/10.1029/97jd00237

Naka, N., & Takemi, T. (2023). Characteristics of the environmental conditions for the occurrence of recent extreme rainfall events in northern Kyushu, Japan. *Scientific Online Letters on the Atmosphere*, *19A*(Special_Edition), 9–19. https://doi.org/10.2151/sola.19a-002

Naka, N., & Takemi, T. (2025). Classifying moist unstable states for the occurrence of precipitation during the summer season in Japan. *International Journal of Climatology*, *45*(10), e8890. https://doi.org/10.1002/joc.8890

NCAR/EOL S-Pol Team. (2023). Precip: NCAR S-Pol radar moments data. Version 1.0 [Dataset]. *UCAR/NCAR–Earth Observing Laboratory*. https://doi.org/10.26023/QA4M-CDHH-MY0Z

NCEP. (2015). NCEP GDAS/FNL 0.25 Degree Global Tropospheric Analyses and Forecast Grids (Updated daily) [Dataset]. *NSF National Center for Atmospheric Research*. https://doi.org/10.5065/D65Q4T4Z

Rasmussen, K. L., & Houze, R. A. (2016). Convective initiation near the Andes in subtropical South America. *Monthly Weather Review*, *144*(6), 2351–2374. https://doi.org/10.1175/mwr-d-15-0058.1

Rasmussen, K. L., & Houze, R. A., Jr. (2012). A flash flooding storm at the steep edge of high terrain: Disaster in the Himalayas. *Bulletin of the American Meteorological Society*, *93*(11), 1713–1724. https://doi.org/10.1175/BAMS-D-11-00236.1

Schumacher, R. S., & Johnson, R. H. (2008). Mesoscale processes contributing to extreme rainfall in a midlatitude warm-season flash flood. *Monthly Weather Review*, *136*(10), 3964–3986. https://doi.org/10.1175/2008MWR2471.1

Skamarock, W. C., Klemp, J. B., Dudhia, J., Gill, D. O., Liu, Z., Berner, J., et al. (2019). *A description of the advanced research WRF model version 4*. NCAR Technical Note NCAR/TN-556+STR.145.

Takemi, T. (2007). Environmental stability control of the intensity of squall lines under low-level shear conditions. *Journal of Geophysical Research*, *112*(D24), D24110. https://doi.org/10.1029/2007JD008793

Takemi, T., & Unuma, T. (2020). Environmental factors for the development of heavy rainfall in the eastern part of Japan during Typhoon Hagibis (2019). *SOLA*, *16*, 30–36. https://doi.org/10.2151/sola.2020-006

Tsuji, H., Takayabu, Y. N., Shibuya, R., Kamahori, H., & Yokoyama, C. (2021). The role of free-tropospheric moisture convergence for summertime heavy rainfall in western Japan. *Geophysical Research Letters*, *48*(18), e2021GL095030. https://doi.org/10.1029/2021gl095030

Wu, Y.-C., Yang, M.-J., & Lin, P.-H. (2020). Evolution of water budget and precipitation efficiency of mesoscale convective systems over the South China Sea. *Terrestrial, Atmospheric and Oceanic Sciences*, *31*(2), 141–158. https://doi.org/10.3319/TAO.2019.07.17.01

Zou, X., Cordeira, J. M., Bartlett, S. M., Kawzenuk, B., Roj, S., Castellano, C., et al. (2023). Mesoscale and synoptic scale analysis of narrow cold frontal rainband during a landfalling atmospheric river in California during January 2021. *Journal of Geophysical Research: Atmospheres*, *128*(20), e2023JD039426. https://doi.org/10.1029/2023JD039426